

Numerical Investigation of Fine particle Transportation and Deposition in the Human Lower Airway: Impact of airflow and particle size on deposition efficiency

Nguyen Dang Khoa

Interdisciplinary Graduate School of Engineering Sciences, Kyushu University

Nguyen Lu Phuong

University of Natural Resources and Environment, Ho Chi Minh City

Ito, Kazuhide

Interdisciplinary Graduate School of Engineering Sciences, Kyushu University

<https://doi.org/10.5109/5909118>

出版情報 : Proceedings of International Exchange and Innovation Conference on Engineering & Sciences (IEICES). 8, pp.366-372, 2022-10-20. Interdisciplinary Graduate School of Engineering Sciences, Kyushu University

バージョン :

権利関係 : Copyright © 2022 IEICES/Kyushu University. All rights reserved.



Numerical Investigation of Fine particle Transportation and Deposition in the Human Lower Airway: Impact of airflow and particle size on deposition efficiency

Nguyen Dang Khoa^{1*}, Nguyen Lu Phuong², Kazuhide Ito¹

¹Interdisciplinary Graduate School of Engineering Sciences, Kyushu University, Japan

²University of Natural Resources and Environment, Ho Chi Minh City, Vietnam

*Corresponding author email: ndkhoa@kyudai.jp

Abstract: Understanding the deposition of inhaled toxic particles is critical in evaluating numerous health risks, especially in the lower airway. Recently, the computational fluid dynamics (CFD) method has been introduced as a promising method to facilitate the accurate prediction of airflow and particle behavior in complex geometry. Therefore, this study applied the CFD method to investigate the deposition characteristic of fine particles in the human respiratory tract from the nostrils to the 7th generation. The airflow pattern was simulated using the Eulerian method at breathing flow rates of 7.5 and 30 L/min, and was followed by particle (aerodynamic diameter 1 to 10 μm) deposition simulation using the Lagrangian method. In general, the results were comparable with experimental data. The high deposited concentration of particles was found at the 5-7th generation, and a specific deposition hot-spot was observed at the carina ridge.

Keywords: Computational fluid dynamics (CFD), human respiratory tract, lower airway, fine particle, deposition fraction.

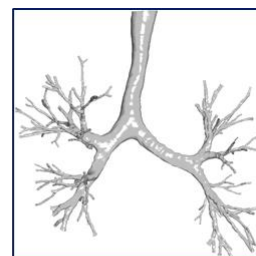
1. INTRODUCTION

The inhalation of airborne particles has raised concerns regarding respiratory-related adverse health effects. Fine particles in indoor environments can be increased due to infiltration from the outdoor environment, originating from indoor sources such as cooking, smoking, building materials, or residents' daily activities [1]. Currently, people spend most of their time (approximately 90%) in enclosed spaces, including homes, schools, and offices. Long-term exposure to inhalable particles can cause asthma, respiratory inflammation, and lung cancer [2]. In particular, lower respiratory infections have been identified as a critical public health problem leading to mortality in all ages [3]. In response, several experimental studies have investigated the deposition of fine particles in the human upper airways [4,5], with results showing the high filter efficiency of the upper airway against larger particle sizes. In-depth studies on particle deposition in the lower airway have also revealed a high concentration of deposited particles [6,7]. Efforts have also been made to construct simulations to predict deposition in human airways using three-dimensional (3D) models segmented from medical images. Among others, our published paper numerically investigated the deposition of a particle in human and monkey upper airways, and concluded that the hotspot of particle deposition for particles larger than 5 μm in diameter was the anterior airway [8,9]. Currently, computer resources facilitate sophisticated studies relating to fluid dynamics in a complex structure such as the human lower airway, and the costly and ethical barriers of experiments on living entities, for example, *in vivo* or *in vitro*, further emphasize the need for numerical simulation utilizing growing computer power [10]. Presently, the computational fluid dynamics (CFD) method has been adopted as a promising alternative that can provide an accurate simulation of airflow in the complex structure of the respiratory tract [11,12], as well as the deposition of virus-laden droplets and viral load [13]. Several simulation efforts have been performed to characterize inhaled particle behavior in the lower airway using a perfect tube-like geometry [14,15], or a realistic model

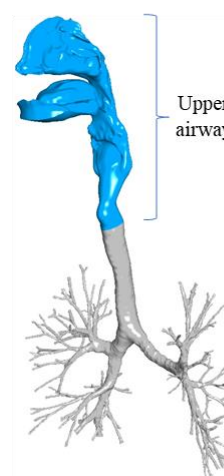
[16,17]. However, morphological and geometric structures and inter-subject variability can result in heterogeneities between individuals during particle deposition. Therefore, this study used the CFD method to investigate the transportation and deposition of fine particles in a realistic human respiratory tract from the nostrils down to the 7th generation of the bronchial tubes under the effects of airflow rates and particle size to contribute to the current knowledge about deposition in the human respiratory tract.



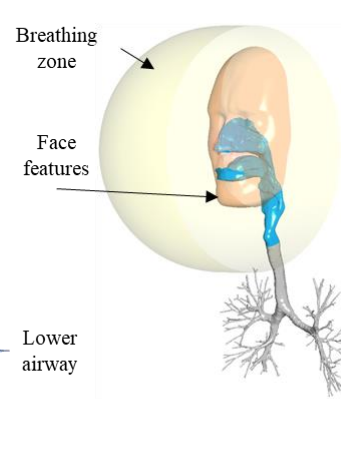
(a) Human lung CT image



(b) Human realistic lower airway up to 7th generation



(c) Human respiratory tract



(d) Computational model

Fig. 1. (a) A representative CT image of the human lower airway. (b) Solid model of the lower airway after extracting from CT images. (c) The respiratory tract from

nostrils to the 7th generation. (d) The outline of computational model.

2. MATERIALS AND METHODS

2.1 Model generation

The realistic lower airway was segmented from computed tomography (CT) data of a healthy and non-smoking adult male volunteer. A representative coronal plane of the human lower airway is shown in Fig. 1a, where the black region denotes the air-filled region and the white region indicates the bony structure. The lower airway includes the trachea and bronchial regions, down to the 7th generation (Fig. 1b). The human respiratory tract was generated by the combination of the upper airway (blue) and segmented lower airway (grey), as shown in Fig. 1c. To create the proper simulation conditions, the external breathing zone and face features were integrated into the respiratory tract, finally forming a complete computational model, as depicted in Fig. 1d.

2.2 Discretization process

The computational domain obtained in the previous section was divided into a set of control volumes using the finite-volume (FVM) method. Herein, poly hexcore elements, a combination of hexa cells in the bulk region and polyhedral cells adjacent to the boundary wall, were adopted, which can reasonably balance the accuracy and computational cost [18], as shown in the cross-sectional plane A-A' (Fig. 2). In addition, 10-prism layers were built adjacent to the boundary wall of the upper airway, which optimized the accuracy of the flow profile in the vicinity of the wall (Fig. 2). For the lower airway, due to the small diameter of the bronchial tubes, 5-prism layers were applied instead.

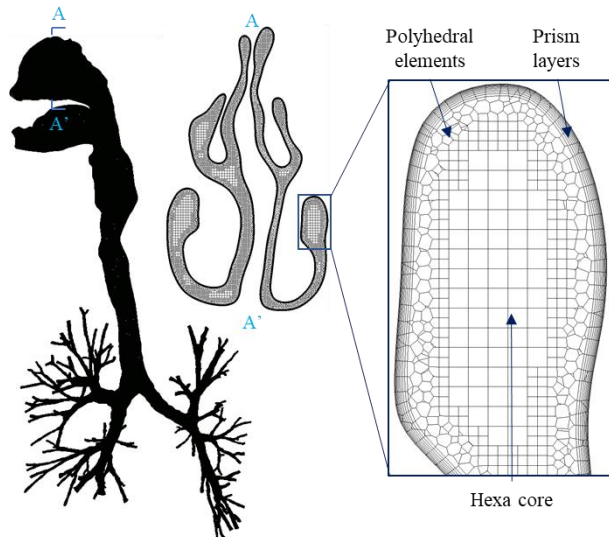


Fig. 2. The mesh design in the respiratory tract. The cross-sectional plane AA' depicts the local mesh design.

2.3 Airflow simulation

We assumed and simulated a steady state, isothermal, and incompressible fluid flow in the respiratory tract using the Eulerian method, in which the set of Reynolds Averaged Navier-Stokes (RANS) equations (Eq. (1) and (2)) were solved computationally for each control volume, as shown in Eq. (1) and (2):

$$\frac{\partial \bar{U}_i}{\partial x_i} = 0 \quad (1)$$

$$\frac{\partial \bar{U}_i}{\partial t} + \frac{\partial}{\partial x_j} (\bar{U}_i \bar{U}_j) = -\frac{1}{\rho_g} \frac{\partial \bar{p}_g}{\partial x_i} + \nu \frac{\partial^2 \bar{U}_i}{\partial x_j^2} - \frac{\partial}{\partial x_j} (\overline{u'_i u'_j}) \quad (2)$$

where \bar{U} represents the ensemble mean velocity; u' represents the fluctuating velocity components; and p_g , ρ , and ν denote the pressure, density, and viscosity of the fluid, respectively. The term Reynolds stresses $\tau_{ij} = \overline{u'_i u'_j}$ states the closure problem to the RANS equation; therefore, the turbulent model was selected to account for the closure problem. This study applied the low-Reynolds-type $k-\varepsilon$ (Abe Kondoh Nagano) turbulent model, which has been shown to provide a reliable prediction of airflow in the respiratory model [11,12]. Different breathing flow rates of 7.5 and 30 L/min were selected to cover the resting and intensive human activities. The numerical boundary conditions are listed in Table 1.

Table 1. Numerical boundary conditions

Parameters	Information
<i>Turbulence model</i>	Low Reynolds type $k-\varepsilon$ model (Abe Kondoh Nagano)
<i>Algorithm</i>	SIMPLE
<i>Convection scheme</i>	Second-order upwind
<i>Inflow boundary</i>	Q = 7.5 and 30 L/min, Turbulent intensity = 10%
<i>Outflow boundary</i>	Gradient zero with Outflow weighting (Table 2)

The human lower airway is geometrically divided into five main regions: the right upper lobe, right middle lobe, right lower lobe, left upper lobe, and left lower lobe [19]. Therefore, the outflow weighting was set differently for each lobe, as performed in a previous study [20] (Table 2).

Table 2. Outflow weighting for each of the lung lobes

Lobes	Flow weighting
<i>Right upper lobe</i>	0.1194
<i>Right middle lobe</i>	0.1089
<i>Right lower lobe</i>	0.3001
<i>Left upper lobe</i>	0.2376
<i>Left lower lobe</i>	0.2349

2.4 Particle deposition simulation

The particle trajectories were predicted using the Lagrangian equation, as shown in Eq. (3).

$$\frac{d\vec{u}_p}{dt} = \vec{F}_D + \vec{F}_G + \vec{F}_S \quad (3)$$

where the subscript p refers to the particle phase, F_G and F_S refer to the gravitational and Saffman lift forces, respectively, and F_D indicates the drag force per particle mass unit.

A total of 50,000 monodispersed particles were introduced into the flow field in front of the nose with an

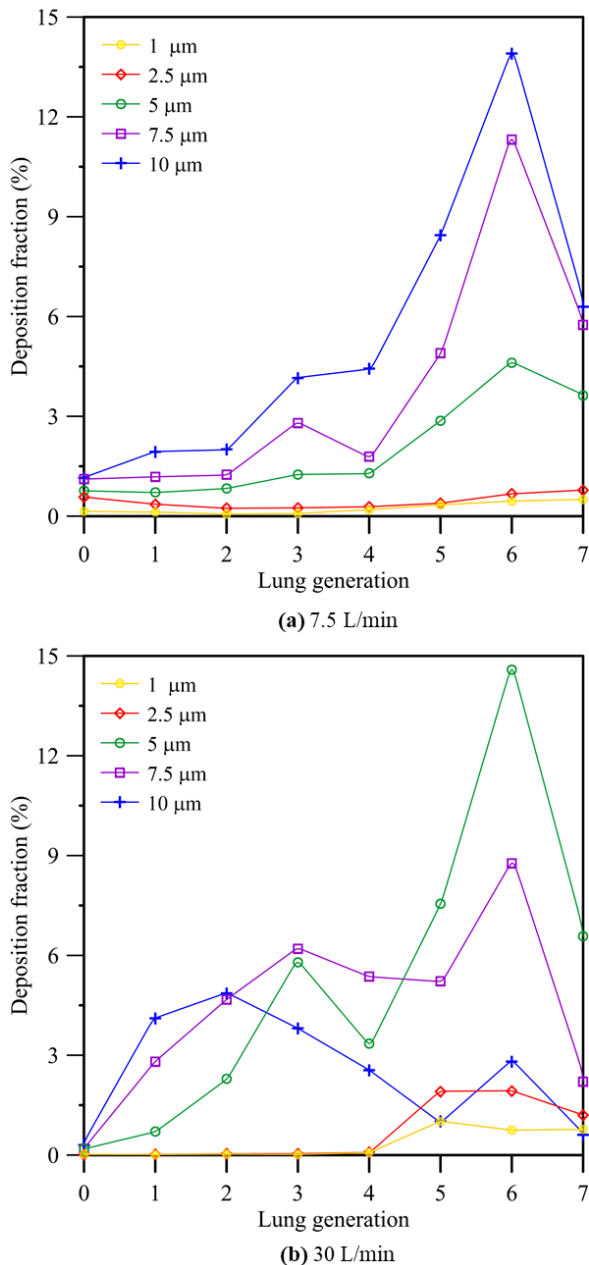


Fig. 3. Validation of the simulated results using the experimental data in the (a) upper airway and (b) lower airway.

initial velocity equal to the fluid velocity at the released position. The aerodynamic diameter of the particles was assigned in the range of 1-10 μm, with a density of 1,000 kg/m³. In the Lagrangian tracking process, a perfect trap condition was assumed for the respiratory walls, which means that the particles had no possibility of rebounding into the flow after hitting the walls.

The total deposition fraction of particles in the respiratory tract is defined as the ratio between the number of particles deposited “ C_{dep} ” and the number of particles entering the respiratory tract “ C_{in} ” (Eq. 4). Accordingly, the local deposition fraction in a specific region i , the specific bronchial tube generation, is defined as the number deposited in region i divided by the total number entering the respiratory tract (Eq. (5)).

$$\eta = \frac{C_{dep}}{C_{in}} \times 100\% \quad (4)$$

$$\eta_i = \frac{C_{dep-i}}{C_{in}} \times 100\% \quad (5)$$

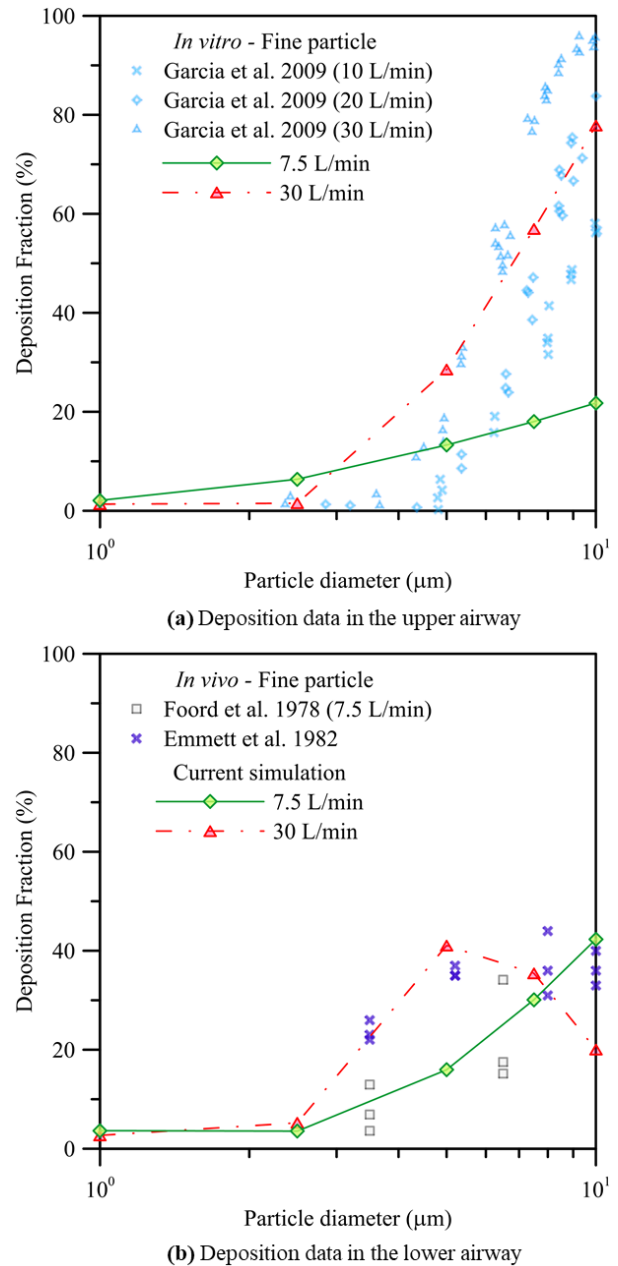


Fig. 4. The local deposition in the lower airway generation at a breathing flow rate of (a) 7.5 L/min and (b) 30 L/min.

3. RESULTS

3.1 Validation of simulated results

The simulated deposition data in the upper and lower airways are plotted as a function of the particle diameter in Fig. 3. For the upper airway, the simulated data were compared with the experimental data obtained from a replica cast (*in vitro*) of the human upper airway [21] (Fig. 3a). The set of *in vivo* data, which was experimentally conducted based on volunteers [6,7], was used to validate the predicted data in the lower airway (Fig. 3b). The simulated results agreed well with the experimental data

in both the upper and lower regions. As shown in Fig. 3a, the deposition fraction increased proportionally with the particle diameter at both breathing flow rates. A higher deposition was observed in the high Reynolds flow (30 L/min), especially for 10 μ m particles (approximately 80%) as compared to 7.5 L/min (around 20%). Meanwhile, in the lower airway, the deposition trend demonstrated heterogeneities between 7.5 and 30 L/min (Fig. 3b), especially for particles larger than 5 μ m. Specifically, the proportional increment of the deposition fraction with particle diameter at a breathing flow rate of 7.5 L/min remained; however, the deposition fraction of 30 L/min showed a decreasing trend from 5 μ m, which means that the highest deposition fraction was recorded at this particle size. For particle sizes of 1-7.5 μ m, a higher deposition rate of 30 L/min persisted compared at 7.5 L/min. Nonetheless, for 10 μ m particles, a lower deposition fraction of 30 L/min (around 20%) was recorded.

3.2 Local deposition fraction in human lower airway

The deposition in each generation at 7.5 and 30 L/min is plotted in Fig. 4. Generation 0 denotes the tracheal region down to the 7th generation. As shown in Fig. 4a, the deposition fraction in the trachea (generation 0) and 1st – 4th generation was low (approximately 3%). The local deposition fraction of particles smaller than 2.5 μ m remained almost constant in the following generations (5th -7th generation). However, the local deposition

fraction rapidly increased in the 5th -7th generation in the case of 5-10 μ m particles, which peaked at the 6th generation. The highest deposition in the 6th generation of 5-10 μ m particles ranged from 4.5% to 13.5%. A decrease in the deposition fraction in the 7th generation was also observed in this particle size range.

For the case of 30 L/min (Fig. 4b), the results show no recorded particles deposited in the tracheal region for all particle sizes, and this phenomenon continued in the 1st – 4th generation in the case of 1 and 2.5 μ m particles. The deposition of these small particles increased in the 5th – 7th generation, but was still lower than 3%. Nonetheless, the local deposition fraction of 5-7.5 μ m demonstrated a discontinuous increment at the 3rd – 5th generations before reaching the highest at the 6th generation with a value of approximately 15% in the case of 5 μ m particles, and that of 7.5 μ m was approximately 9%. A decrement trend is also observed in the 7th generation of 5 and 7.5 μ m particles, similar to the results of 7.5 L/min. Interestingly, the local deposition characteristic of 10 μ m particles portrayed apparent discrepancies compared to the others. In particular, the highest deposition was recorded in the 2nd generation (approximately 4.5%) before gradually decreasing in the following generations and was the lowest in the 5th generation (about 1.5%). A slight fluctuation in the 6th and 7th generation was also observed.

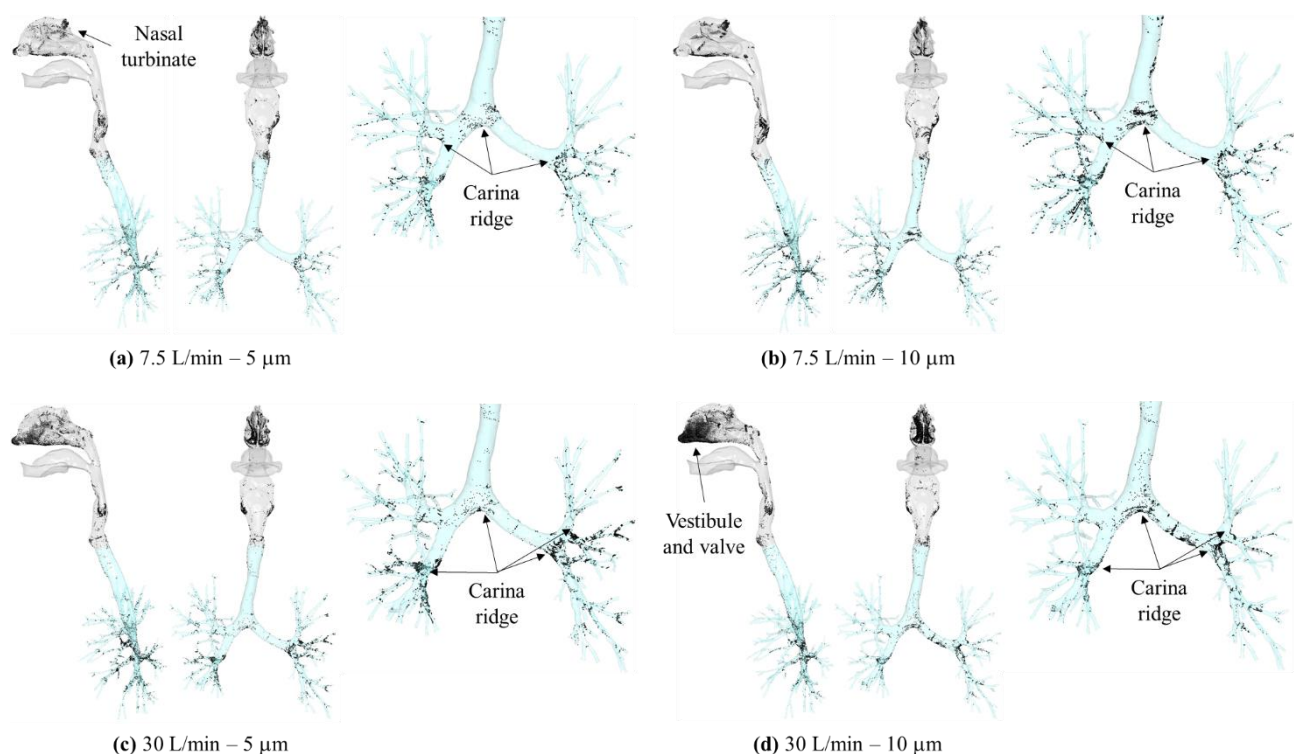


Fig. 5. Visualization of deposited particle in the human respiratory tract including the upper airway (transparent grey) and lower airway (transparent blue) in the (a, b) 7.5 L/min and (c, d) 30 L/min.

3.3 Visualization of the deposited particles in the human respiratory tract

A 3D visualization of the particles deposited in the respiratory tract is depicted in Fig 5. In general, the deposition of large particles accumulated at a specific

position rather than covering the entire inner airway surface. In particular, hot-spots of 5 and 10 μ m deposited particles were observed identically in the nasal turbinate region of the upper airway at 7.5 L/min (Figs 5a and 5b). In the lower airway, the particles tended to deposit in the

carina ridge, where the airflow was separated into two streams. The same phenomena were recorded for the 5 and 10 μm particles (Figs 5a and 5b).

At 30 L/min, a high concentration of particles accumulated in the upper airway; however, the vestibule and valve region accounted for the higher deposition than the nasal turbinate region at 7.5 L/min (Figs 5c and 5d). Nonetheless, the focal point of the particles in the lower airway shared common characteristics between 7.5 and 30 L/min.

4. DISCUSSIONS

The CT-based CFD method can provide promising outcomes for studies involving health risk assessment in the human respiratory tract. In this study, we conducted a numerical simulation of airflow patterns and fine particle deposition in the human respiratory tract, with the main focus on the lower airway region. The complex and nonlinear behavior of particles in the lower airway can be quantitatively described, and the local deposition fraction in each generation can be quantitatively analyzed. Visualizing the particle hotspot in the lower region can facilitate further studies relating to drug delivery and the control of adverse health effects due to exposure to respirable particles.

The validation results demonstrated the reliability of the CFD method for simulating particle deposition in the human respiratory tract. The higher deposition of 10 μm particles in the upper airway at 30 L/min is due to inertia impaction being the main deposition scheme for particles with diameter $>2\ \mu\text{m}$ in the upper airways, as stated in a previous study [22]. Thus, the higher the Reynolds flow, the higher the inertial effects, resulting in higher deposition. Researchers have previously concluded that inertia impaction is also the governing force of fine particle deposition in the lower airway with a diameter $>3\ \mu\text{m}$ [23]. Therefore, a higher Reynolds flow and larger particle diameter would theoretically yield higher deposition in the lower airway. However, as shown in the results, the decrease in the deposition fraction as the particle size increased in the case of 30 L/min was attributed to the fact that most larger particles ($d>7.5\ \mu\text{m}$) were trapped in the upper airway, leading to fewer particles entering the lower airway. In contrast, the lower deposition in the upper airway at 7.5 L/min allowing more particles to penetrate the lower airway, and a continuous increment in the deposition fraction following the particle size in the lower airway was achieved. As can be seen, both the upper and lower respiratory tracts (down to the 7th generation) play an important role in filtering the fine particles; if the particles can pass the filtration mechanism of the upper airway, then there is a high possibility of being removed from the airstream by the lower airway as compensation.

Deposition in the human lung is strongly affected by biological factors, including lung morphometry, breathing patterns, fluid dynamics, and particle properties [24]. Evidently, the previous simulation effort conducting the deposition of particles in artificial human lung airways revealed the highest deposition in the 5th generation in the case of 5 μm , and that of 10 μm was 2nd generation for 70 years old human; however, as age

decreased, the peak generation shifted to the 6th and 4th generations for 5 and 10 μm particles, respectively [25]. Therefore, the local deposition phenomena in this study reflects the current individual structural features of the lung models segmented from CT images and other simulation initial conditions, rather than the universal deposition phenomena. The highest deposition in the 6th generation was the main deposition feature in the current lower airway. As mentioned above, the inertia impaction governs the deposition of particles in the lower airway, which is responsible for the higher deposition of high-inertia particles (5-10 μm) compared to low-inertia particles (1-2.5 μm) in the case of 7.5 L/min. It is noteworthy that although the inertia impaction is even more applicable, the singularities of the deposition trend of high-inertia particles in the case of 30 L/min is attributed to the impacts of upper airway deposition, which performs its efficient filtering mechanism. Thus, simulation studies involving health risk assessment or drug delivery in the human lung should consider the coupled deposition of both the upper and lower airways rather than the lower airway itself.

Under the effects of inertia impaction, the deposition of particles was highest in the vestibule, vale, and nasal turbinate regions, because the acceleration of airflow and complex structure in these regions hampered the smooth movement of particles, as shown in our previously published work [9]. These results agree with those reported in several published papers regarding the deposition of fine particles in the upper airway [26,27]. The focal point of the deposition at the carina ridge again highlights the effects of inertial impaction, in which it is difficult for the high-inertia particles to change their original direction adapting to the flow at the branching position. Previous simulation efforts also observed and confirmed these phenomena [28,29]. Therefore, the high accumulation at the carina ridge can be considered as the universal deposited characteristic of large particles in the human lower airway, despite the factors related to airway structural discrepancies or inter-subject variability.

5. CONCLUSIONS

A realistic human airway from the nostrils down to the 7th generation was successfully generated from CT images, which explicitly describes its nature and complex structure. The CFD method was applied to predict the airflow patterns and particle deposition. The coupling between image processing and the CFD method provided a promising outcome to assess the health risks associated with the inhalation of foreign airborne particles. The deposition in the lower airway is significantly affected by the upper airway, which indicates that the extremely high deposition in the upper region could minimize the deposition in the lower region in the high inertia impaction case (30 L/min and 5-10 μm particles). In contrast, the upper and lower airways showed a low filtration efficiency against small particles ($d<2.5\ \mu\text{m}$). The current study revealed the highest deposition in the 6th generation in almost all investigated cases, except for the 10 μm particles at 30 L/min, where the 2nd generation accounted for the highest deposition.

Notably, the carina ridge was found to be the focal point of the accumulated particles. Therefore, drug delivery studies or health risk assessments involving the lower airway should consider the carina ridge region. The present study contributes to the current knowledge on particle deposition in the lower airway. However, some limitations, including the restrictive number of generation orders (only up to the 7th generation) and the absence of a cyclic breathing process, should be mentioned.

FUNDING SOURCES

This research was partially funded by the Japan Science and Technology (JST), CREST Japan (grant number JP 20356547), and the Japan Society for the Promotion of Science (JSPS) Grants-in-Aid for Scientific Research (KAKENHI) (grant numbers JP 22H00237 and JP 20KK0099), Health Labour Sciences Research Grant (JP 21KD2002), MEXT as “Program for Promoting Researches on the Supercomputer Fugaku” (JPMXP1020210316). The computation was partially performed using the computer resources offered under the category of Intensively Promoted Projects by the Research Institute for Information Technology, Kyushu University.

6. REFERENCES

- [1] A. C. K. Lai, W. W. Nazaroff, Modeling indoor particle deposition from turbulent flow onto smooth surfaces, *J. Aerosol Sci.* 31 (2000) 463–476.
- [2] Y.-F. Xing, Y.-H. Xu, M.-H. Shi, Y.-X. Lian, The impact of PM_{2.5} on the human respiratory system, *Journal of Thoracic Disease*, vol. 8, no. 1, p. 6, 2016.
- [3] C. Troeger, M. Forouzanfar, P. C Rao, I. Khalil, A. Brown, S. Swartz, N. Fullman, J. Mosser, R. L Thompson, R. C Reiner, A. Abajobir, N. Alam, M. A. Alemayohu, A. T Amare, C. A. Antonio, H. Asayesh, E. Avokpaho, A. Barac, M. A Beshir, D. Jara Boneya, M. Brauer, L. Dandona, R. Dandona, J. R A Fitchett, T. T. Gebrehiwot, G. B. Hailu, P. J Hotez, A. Kasaeian, T. Khoja, N. Kissoon, L. Knibbs, G. A. Kumar, R. K. Rai, H. M. Abd El Razek, M. S K Mohammed, K. Nielson, E. Oren, A. Osman, G. Patton, M. Qorbani, H. S. Roba, B. Sartorius, M. Savic, M. Shigematsu, B. Sykes, S. Swaminathan, R. Topor-Madry, K. Ukwaja, A. Werdecker, N. Yonemoto, M. El Sayed Zaki, S. S Lim, M. Naghavi, T. Vos, S. I Hay, C. J L Murray, A. H Mokdad, Estimates of the global, regional, and national morbidity, mortality, and aetiologies of lower respiratory tract infections in 195 countries: a systematic analysis for the Global Burden of Disease Study 2015, *Lancet Infect. Dis.* 17 (2017) 1133–1161.
- [4] J. T. Kelly, B. Asgharian, J. S. Kimbell, B. A. Wong, Particle Deposition in Human Nasal Airway Replicas Manufactured by Different Methods. Part I: Inertial Regime Particles, *Aerosol Sci. Technol.* 38 (2004) 1063–1071.
- [5] D.-J. Hsu, M.-H. Chuang, In-Vivo Measurements of Micrometer-Sized Particle Deposition in the Nasal Cavities of Taiwanese Adults, *Aerosol Sci Technol.* 46 (2012) 631–638.
- [6] N. Foord, Black. M. Walsh, Regional deposition of 2.5-7.5 micrometer diameter inhaled in healthy male non-smokers, *J. Aerosol Sci.* 9 (1978) 343–357.
- [7] P. C. Emmett, R. J. Aitken, W. J. Hannan, Measurements of the total and regional deposition of inhaled particles in the human respiratory tract, *J. Aerosol Sci.* 13 (1982) 549–560.
- [8] N. Lu Phuong, N. Dang Khoa, K. Inthavong, K. Ito, Particle and inhalation exposure in human and monkey computational airway models, *Inhalation Toxicology*. 30 (2018) 416–428.
- [9] N. L. Phuong, N. D. Khoa, K. Ito, Comparative numerical simulation of inhaled particle dispersion in upper human airway to analyse intersubject differences, *Indoor and Built Environ.* 29 (2020) 793–809.
- [10] K. Ito, An in silicon human model for fluid-initiated environmental design in an enclosed space, in *Proceedings of International Exchange and Innovation Conference on Engineering & Sciences (IEICES)*, Oct. 2017, vol. 3, pp. 13–14.
- [11] N. L. Phuong, K. Ito, Investigation of flow pattern in upper human airway including oral and nasal inhalation by PIV and CFD, *Building and Environ.* 94 (2015) 504–515.
- [12] N. L. Phuong, T. V. Quang, N. D. Khoa, J.-W. Kim, K. Ito, CFD analysis of the flow structure in a monkey upper airway validated by PIV experiments, *Respiratory Physiology and Neurobiology*. 271 (2020) 103304.
- [13] H. Li, K. Kuga, Nguyen Dang Khoa, K. Ito, Effects of Initial Conditions and Parameters on the Prediction of SARS-CoV-2 Viral Load in the Upper Respiratory Tract Based on Host-Cell Dynamics, in *Proceedings of International Exchange and Innovation Conference on Engineering & Sciences (IEICES)*, Oct. 2021, vol. 7, pp. 155–160.
- [14] A. Fernández Tena, P. Casan Clarà, Deposition of Inhaled Particles in the Lungs, *Archivos de Bronconeumología (English Edition)*. 48 (2012) 240–246.
- [15] M. S. Islam, S. C. Saha, E. Sauret, T. Gemci, Y. T. Gu, Pulmonary aerosol transport and deposition analysis in upper 17 generations of the human respiratory tract, *J. Aerosol Sci.* 108 (2017) 29–43.
- [16] D. Li, Q. Xu, Y. Liu, Y. Libao, J. Jun, Numerical Simulation of Particles Deposition in a Human Upper Airway, *Advances in Mechanical Engineering*. 6 (2014) 207938.
- [17] J. Dong, Y. Shang, L. Tian, K. Inthavong, D. Qiu, J. Tu, Ultrafine particle deposition in a realistic human airway at multiple inhalation scenarios, *Int. J. Numer. Meth. Biomed. Engng.* 35 (2019) e3215.
- [18] K. Zore, G. Parkhi, B. Sasanapuri, A. Varghese, 21th Annual CFD Symposium, August 8-9, 2019, Bangalore, in *Annual CFD Symposium*, Aug. 2019, pp. 0–11.
- [19] E. Weibel, *Morphometry of the Human Lung*. Springer-Verlag Berlin Heidelberg GmbH, 1963.
- [20] D. A. Shelley, B. L. Sih, and L. J. Ng, An integrated physiology model to study regional lung damage effects and the physiologic response, p. 19, 2014.

- [21] G. J. M. Garcia, E. W. Tewksbury, B. A. Wong, and J. S. Kimbell, Interindividual Variability in Nasal Filtration as a Function of Nasal Cavity Geometry, *J. Aerosol Med. Pulm. Drug Deliv.* 22 (2009) 139–156.
- [22] C. Darquenne, Deposition Mechanisms, *J. Aerosol Med. Pulm. Drug Deliv.* 33 (2020) 181–185.
- [23] C. Ou, J. Hang, Q. Deng, Particle Deposition in Human Lung Airways: Effects of Airflow, Particle Size, and Mechanisms, *Aerosol Air Qual. Res.* 20 (2020) 2846–2858.
- [24] W. Hofmann, Modelling inhaled particle deposition in the human lung—A review, *J. Aerosol Sci.* 42 (2011) 693–724.
- [25] Md. M. Rahman, M. Zhao, M. S. Islam, K. Dong, S. C. Saha, Aging effects on airflow distribution and micron-particle transport and deposition in a human lung using CFD-DPM approach, *Advanced Powder Technology.* 32 (2021) 3506–3516.
- [26] P. Farhadi Ghalati, E. Keshavarzian, O. Abouali, A. Faramarzi, J. Tu, A. Shakibafard, Numerical analysis of micro- and nano-particle deposition in a realistic human upper airway, *Computers in Biology and Medicine.* 42 (2012) 39–49.
- [27] H. Calmet, C. Kleinstreuer, G. Houzeaux, A.V. Kolanjiyil, O. Lehmkuhl, E. Olivares, M. Vázquez, Subject-variability effects on micron particle deposition in human nasal cavities, *J. Aerosol Sci.* 115 (2018) 12–28.
- [28] L. Tian, G. Ahmadi, Transport and Deposition of Micro-and Nano-Particles in Human Tracheobronchial Tree by an Asymmetric Multi-Level Bifurcation Model, *The Journal of Computational Multiphase Flows.* 4 (2012) 159–182.
- [29] P. K. Rajaraman, J. Choi, E. A. Hoffman, P. T. O'Shaughnessy, S. Choi, R. Delvadia, A. Babiskin, R. Walenga, C.-L. Lin, Transport and deposition of hygroscopic particles in asthmatic subjects with and without airway narrowing, *J. Aerosol Sci.* 146 (2020) 105581.